Contrast-dependent phase sensitivity in area MT of macaque visual cortex

Shaun L. Cloherty[a,b,c,d] and Michael R. Ibbotson[a,b]

In primate visual cortex (V1), about half the neurons are sensitive to the spatial phases of grating stimuli and generate highly modulated responses to drifting gratings (simple cells). The remaining cells show far less phase sensitivity and relatively unmodulated responses to moving gratings (complex cells). In the second visual area (V2) and the motion processing area MT (or V5), the majority of cells have unmodulated responses to drifting gratings – they are phase invariant. At just-detectable contrasts, 44% of V1 complex cells show highly modulated responses, but this contrast-dependent phase sensitivity is found in only 7% of V2 complex cells. We recorded from 149 cells in macaque MT – 142 classed as complex cells at high contrast. Approximately 14% (20/142) of MT complex cells showed significantly modulated responses to drifting gratings at just-detectable contrasts. A general feature of MT cells is that they can be divided into pattern and component selective types, but we found no correlation between this classification and contrast-dependent phase sensitivity. Phase sensitivity in MT is discussed in relation to MT's input structure. *NeuroReport* **30:195–201 Copyright © 2019 Wolters Kluwer Health, Inc. All rights reserved.**

NeuroReport 2019, **30**:195–201

Keywords: macaque cortex, motion processing, visual system

[a]National Vision Research Institute, Australian College of Optometry, Carlton, [b]ARC Centre of Excellence for Integrative Brain Function, Department of Optometry and Vision Sciences, University of Melbourne, Parkville, [c]Department of Physiology and [d]Biomedicine Discovery Institute, Monash University, Clayton, Victoria, Australia

Correspondence to Michael R. Ibbotson, BSc, PhD, National Vision Research Institute, Australian College of Optometry, Cnr Cardigan and Keppel Streets, Carlton, VIC 3053, Australia
Tel: + 61 393 497 481; fax: + 61 393 497 559; e-mail: mibbotson@nvri.org.au

Received 14 October 2018 **accepted** 4 December 2018

Introduction

At high contrast, approximately half of the neurons in the primate primary visual cortex (V1) are selective for the spatial phases of grating stimuli (simple cells), whereas the rest (complex cells) are phase invariant [1,2]. Most of the input to the second visual area (V2) arises from V1, but only 13–25% of V2 neurons (depending on eccentricity) are simple cells – most have complex-like responses [3]. This is despite V2's input from V1 being dominated by phase-sensitive simple cells [4]; thus, there must be a high degree of spatial summation between areas. At high contrast, complex cells are phase invariant, but when very close to the contrast threshold, 44% of V1 cells, but only 7% of V2 cells, show phase-sensitive response characteristics [5].

Here, we investigate the effect of stimulus contrast on the observed phase sensitivity of cells in primate area MT and compare it with V1 and V2. MT is interesting in this respect because its neurons summate inputs in complex ways, for example, they are direction selective [6], receive input from many brain areas [7,8], and have larger receptive fields (RFs) than neurons in afferent regions [9]. The expectation was that MT would show little sign of contrast-dependent phase sensitivity. Contrary to expectations, we found that 14% (20/142) of MT complex cells showed significantly increased levels of phase sensitivity at threshold contrast. Given the recent interest in subcortical inputs to MT, which may explain its ability to respond when V1 is inactivated [10], along with recent models of MT that suggest a nonhierarchical processing mechanism [11,12], we believe that MT's contrast-dependent phase-sensitive characteristics need to be further explored.

Materials and methods

Electrophysiology

We recorded extracellular spiking responses from 149 well-isolated single units in area MT from five monkeys (*Macaca fascicularis*, 4.3–4.7 kg). Using identical techniques, we also recorded from V1 ($n = 166$) and V2 ($n = 134$) in a further six macaques, but the results from those animals have been published previously, and are presented here to facilitate a direct comparison [5]. Surgical and experimental procedures conformed to the NIH Guide for the Care and Use of Laboratory Animals and were approved by the Animal Welfare Committee at New York University.

A craniotomy, ~10 mm in diameter, was performed 10 mm posterior to interaural zero and 12 mm lateral to the midline. Extracellular recordings were made using quartz/platinum–tungsten microelectrodes (Thomas Recording GmbH, Giessen, Germany). Electrodes penetrated the surface of V1 ~6 mm behind the lunate sulcus and 15–16 mm lateral to the midline, and advanced in the rostral direction (20° from horizontal) within a parasagittal plane. Electrodes traversed the gray matter in V1, followed by a region of white matter (characterized by an absence of spiking activity) before entering the gray matter in V2 on the posterior bank of the lunate sulcus. Electrodes passed through the lunate sulcus and entered the posterior bank of the superior

DOI: 10.1097/WNR.0000000000001183

temporal sulcus (8–12 mm from the surface of V1). Area MT was identified by recording depth relative to the V1 surface and its direction-selective responses. RFs in MT were centered within 11° of the fovea (>90% centered within 7°). Signals were amplified, bandpass-filtered (300–10 kHz), and sampled with 16-bit precision (25 kHz). Single units were isolated online using dual-window time-amplitude discrimination software (Expo; P. Lennie, University of Rochester, Rochester, New York, USA). Spike times were saved with a temporal resolution of 0.1 ms. After the experiments, the monkeys were killed with an overdose of sodium pentobarbital.

Visual stimuli and data acquisition

Visual stimuli were generated by a computer running Expo (Apple Macintosh; Apple Inc., Cupertino, California, USA). Stimuli were presented on a calibrated monitor [Eizo FlexScan T966 CRT (EIZO Corporation, Hakusan, Ishikawa, Japan); resolution: 1280 × 960 pixels; refresh rate: 120 Hz]. The monitor was placed 114 cm from each monkey's eyes (subtending 20° × 15°; mean luminance: 31.2 cd/m^2). For each cell, we mapped the RF through each eye using bright or dark bars and a small circular patch of moving sine-wave grating. After determining the eye that produced the largest response, all subsequent stimuli were centered on its RF and the other eye was occluded. Stimuli consisted of luminance modulated sine-wave gratings and plaids, presented on a mean gray background within a soft-edged circular aperture. Recordings began by measuring the optimal motion direction, spatial frequency, temporal frequency, and size of the grating for each cell. We then measured the responses to optimal moving sine-wave gratings of 10 different Michelson contrasts (0.01–1.0). Gratings or plaids and a blank (mean gray) condition were presented for 1 s, interleaved in a block pseudorandom order, with no interstimulus interval.

Analysis of neuronal responses

The mean firing rate for each stimulus condition was computed within a 1 s window. The onset of this window was chosen to maximize the variance across all stimulus conditions, including the blank condition [13]. We discarded responses to the first cycle of each stimulus to remove onset transients [14], and then cycle-averaged the responses to each stimulus condition across trials. Spontaneous activity was the mean spike count during the blank condition. At each contrast, we quantified the phase sensitivity of the cell by calculating the relative modulation – F_1/F_0 – of the responses as the amplitude of the Fourier component at the fundamental frequency of the grating stimulus (F_1) divided by the mean response (F_0) after subtraction of the spontaneous rate [15].

Relative modulation of the observed responses at high and low contrasts was compared. The high-contrast condition, by definition, induced the maximum response (usually 100% contrast). Low contrast was defined as the lowest contrast that generated a response significantly above the cell's spontaneous rate. This low-contrast condition was determined using a receiver operating characteristic curve analysis [5]. Because of differences in each cell's contrast sensitivity, the low-contrast condition was different for each cell in the population.

Increase in F_1/F_0 with reduced spike count

Fourier analysis of spike trains is influenced by the number of spikes collected [16,17]. For each cell, we compared the observed F_1/F_0 with an empirical distribution of F_1/F_0 derived from a model complex cell. This enabled us to estimate the increase in F_1/F_0 that could be explained by the reduction in the number of spikes recorded at low contrast. The model cell generates n spikes per cycle of an optimal sine-wave grating (response interval T). Spike arrival times, $t_i \in [(-\pi,\pi), i = 1 \ldots n$, are assumed to be independent identically distributed random variables drawn from a raised cosine distribution defined by:

$$f(t;A,B) = \frac{1}{2\pi}\lfloor 1 + A\cos(t-B)\rfloor \quad B-\pi \le t < B+\pi, \tag{1}$$

where $0 \le A \le 1$ defines the assumed true or asymptotic F_1/F_0 (i.e. the expected value of F_1/F_0 as $n \to \infty$, denoted as $\langle F_1/F_0\rangle_\infty$) and B defines the position of the distribution. For a perfect phase-invariant complex cell, $A = 0$ [i.e. Eq. (1) reduces to the uniform distribution]. To simulate responses with a given asymptotic $\langle F_1/F_0\rangle_\infty$, we set $A = \langle F_1/F_0\rangle_\infty$ and $B = 0$.

We maximized the likelihood of the data observed to determine the appropriate $\langle F_1/F_0\rangle_\infty$ for each cell, that is, we computed the log likelihood L of the data for a given asymptotic F_1/F_0 as follows:

$$\log L = \log \prod\nolimits_j f(A_n \mid A), \tag{2}$$

where A_n is F_1/F_0 of the cell on the basis of the observed response containing n spikes, A is the specified asymptotic level of response modulation [from Eq. (1)], and j is an index indicating the contrast that generates the maximum response.

For each cell, distributions of F_1/F_0 were computed at spike counts (n) corresponding to the number of spikes recorded for the lower stimulus contrasts. This was done after choosing the asymptotic F_1/F_0 for the model to maximize the likelihood of the data observed at maximum contrast. From these distributions, we calculated 99% confidence limits for the increase in F_1/F_0 expected simply because of the reduction in the number of spikes recorded. The increase in F_1/F_0 at low contrast must exceed the 99% confidence limit of the corresponding empirical distribution of F_1/F_0 for it to be considered significant.

Results

Extracellular recordings were made from 149 neurons in area MT. Of these, 142 (95.3%) were complex cells and seven (4.7%) were simple cells, as defined at 100% contrast. Using accepted methods [5], the phase sensitivities of the MT neurons were assessed on the basis of their responses to optimal moving sine-wave gratings over a range of stimulus contrasts.

We compared F_1/F_0 observed at high contrast with that observed at threshold contrast for all cells. Figure 1a shows F_1/F_0 at the lowest contrast that produced a significant response, plotted against F_1/F_0 at high contrast for 149 MT neurons. The simple cells did not show consistent or significant changes in F_1/F_0 with contrast. From the complex cells, 20/142 (14%) showed a significant increase in F_1/F_0 (black symbols in Fig. 1a). Figure 1b and c show comparable data for 133 and 166 cells from V2 and V1, respectively. At high contrasts, it is evident that most MT and V2 complex cells have F_1/F_0 less than 0.5. In contrast, V1 cells have a wide spectrum of modulation ratios, with half the cells showing simple cell properties and half showing complex cell phase sensitivities (Fig. 1c). At low contrast, it is evident that many V1 cells show an increase in F_1/F_0 (Fig. 1c). In MT and V2, far fewer cells show a significant increase in phase sensitivity at low contrast (Fig. 1a and b).

We show the distributions of threshold contrasts for all complex cells in MT (Fig. 2a), V2 (Fig. 2b), and V1 (Fig. 2c). In these, and subsequent figures, black bars show the distributions for cells that showed a significant increase in F_1/F_0 at low contrast, whereas gray bars show data for all complex cells. These distributions deviate from normal (Lilliefors' goodness-of-fit test, $P > 0.05$). Although the distributions for V1 and V2 are indistinguishable (two-sample Kolmogorov–Smirnov goodness-of-fit test, $P = 0.75$), the distribution for MT showed significantly greater sensitivity to low stimulus contrasts (Kolmogorov–Smirnov goodness-of-fit test, $P < 0.001$).

We present several population measures for MT (Fig. 3a), V2 (Fig. 3b), and V1 (Fig. 3c). The upper row shows the distribution of F_1/F_0 for the three cortical areas and highlights the clear dominance of cells with low response modulation in areas MT and V2. The second row shows the distribution of F_1/F_0 obtained from the same cells at near-threshold contrast. The third row shows the change in F_1/F_0 for all cells in all three cortical areas and the bottom row shows the deviation from the expected change in F_1/F_0 (on the basis of reduced spike count). MT cells showed an increase in F_1/F_0 at threshold contrasts of 0.12 (two-sided Wilcoxon signed rank test, $P < 0.001$) (Fig. 3a). Cells in V2 showed a small increase in F_1/F_0 at threshold contrasts of 0.08 (two-sided Wilcoxon signed rank test, $P < 0.001$) (Fig. 3b). Cells in V1 showed a median increase in F_1/F_0 of 0.32 (two-sided Wilcoxon signed rank test, $P < 0.001$) (Fig. 3c). These measures do not account for changes in the observed spike counts. When controlling for the change in spike count when testing at threshold contrasts (see the Materials and methods section), only V1 shows a significant increase in F_1/F_0 (median: 0.24; two-sided Wilcoxon signed rank test, $P < 0.001$; Fig. 3c, bottom). Area V2 showed no

Fig. 1

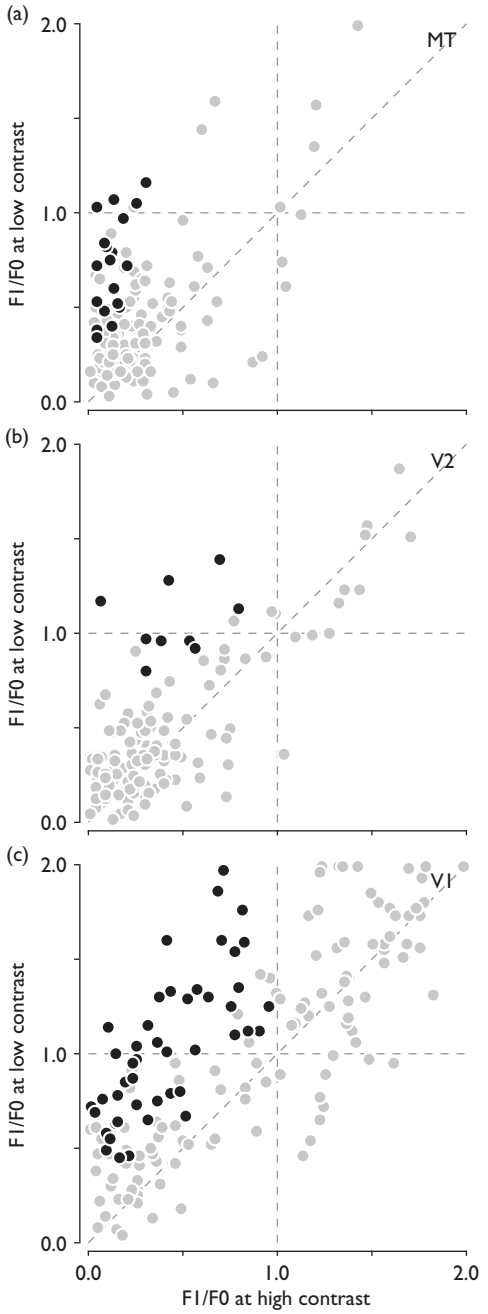

Relative modulation (F_1/F_0) of responses at low compared to high stimulus contrast. (a) Scatter plot of F_1/F_0 observed at threshold contrast plotted against F_1/F_0 observed at high contrast for 149 cells in area MT. Each symbol represents a single cell. (b, c) Similar data for 134 cells in V2 and 166 cells in V1, respectively (data in b, c are from Cloherty and Ibbotson [5]). Complex cells showing a significant ($P < 0.01$) increase in F_1/F_0 at threshold contrast are shown in black. All the remaining cells (simple and complex) are shown in gray.

Fig. 2

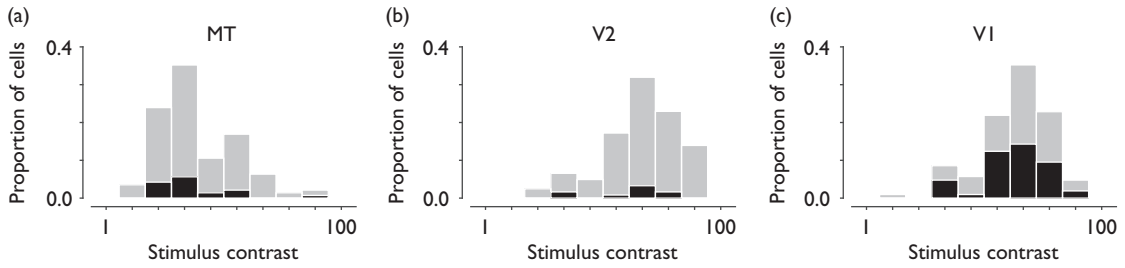

Distributions of threshold stimulus contrast – the lowest stimulus contrast that induced a significant response (based on the receiver operating characteristic curve analysis). (a) Distribution of threshold contrast for 142 complex cells in MT. (b, c) Comparable distributions for complex cells in V2 (122 cells) and V1 (105 cells), respectively. Black bars show the distributions for the subset of complex cells showing a significant increase in F_1/F_0 at low contrast. Gray bars show the distribution for all other complex cells.

Fig. 3

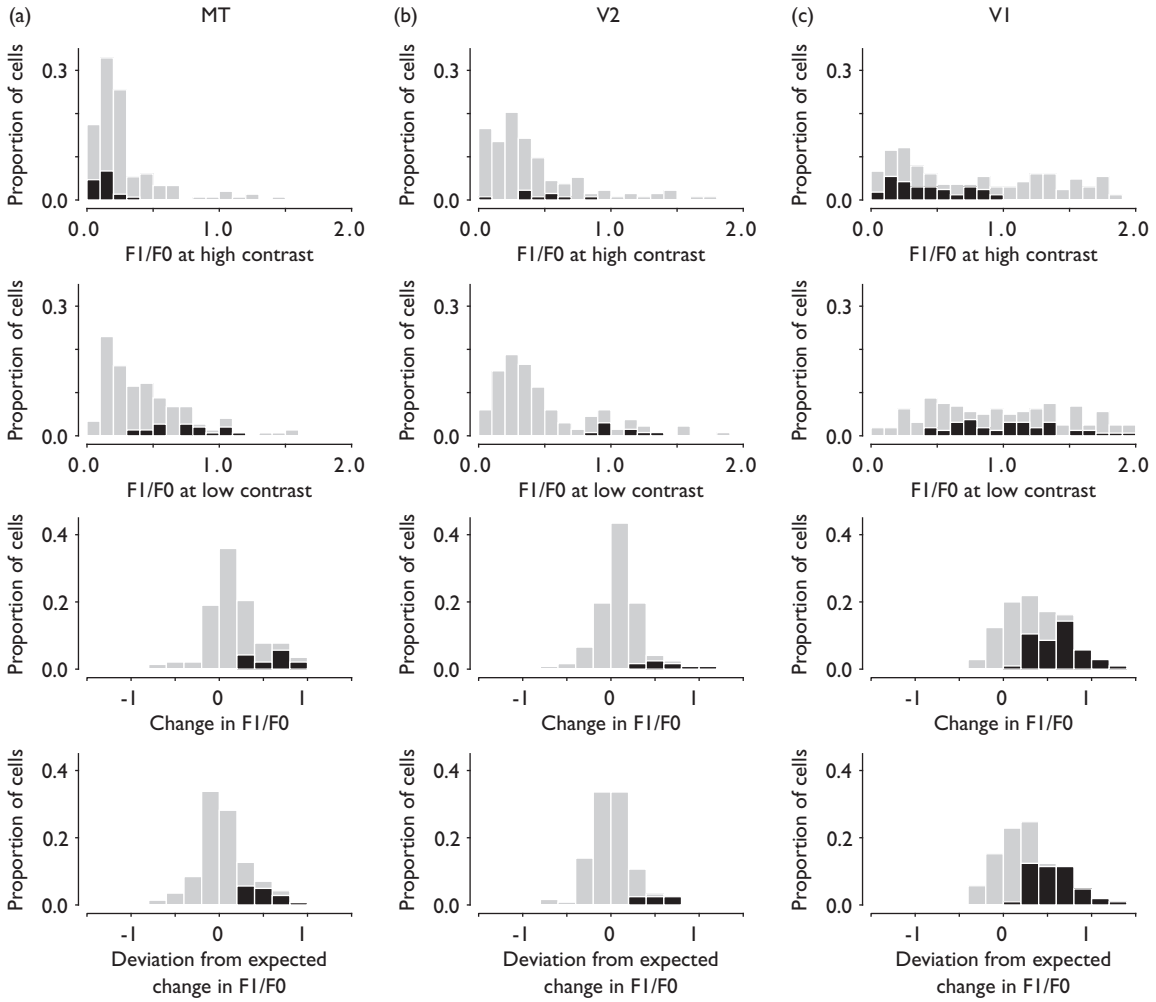

Changes in F_1/F_0 with stimulus contrast. (a) Histograms of the change in F_1/F_0 at threshold contrast compared with that at high contrast for complex cells in MT. (b, c) Similar distributions for complex cells in V2 and V1, respectively. Black bars show the distributions for the subset of complex cells showing a significant increase in F_1/F_0 at low contrast. Gray bars show the distribution for all other cells. In each panel, histograms show (from top to bottom) F_1/F_0 at high contrast, F_1/F_0 at low contrast, the change in F_1/F_0 at low contrast compared with high contrast, and the deviation from the expected change in F_1/F_0 on the basis of reduced spike count alone.

change in F_1/F_0 at the population level (median: -0.005; two-sided Wilcoxon signed rank test, $P=0.99$; Fig. 3b, bottom). Area MT showed a small but not significant increase in F_1/F_0 at the population level (median: 0.03; two-sided Wilcoxon signed rank test, $P=0.07$; Fig. 3a, bottom).

Although we did not observe significant changes in F_1/F_0 with stimulus contrast in V2 or MT at the population level, we did observe a difference between the two areas. In V2, the mean F_1/F_0 of those cells that showed contrast-dependent phase sensitivity was 0.46 ± 0.22 ($n=9$) at high contrast and 1.06 ± 0.19 at low contrast. Even at high contrast, these cells had relatively high phase sensitivity compared with most V2 cells (Fig. 3b). Conversely, the MT cells that showed contrast-dependent phase sensitivity had mean F_1/F_0 values at high and low contrasts of 0.13 ± 0.07 and 0.73 ± 0.25 ($n=20$), respectively. Thus, these MT cells were very phase insensitive at high contrast. This is evident when comparing the histograms at the top of Fig. 3a and b, showing the distribution of F_1/F_0 for these cells (black bars) in MT and V2.

For all but five of our MT cells, we also recorded responses to moving plaid patterns in addition to the standard grating stimuli. We classified these cells as either pattern or component selective (or unclassified) on the basis of the partial correlation between their responses to plaid stimuli and predicted pattern and component selective responses derived from their direction tuning curves for the component gratings alone [18]. From 138 MT complex cells, 41 were pattern selective, 56 were unclassified, and 41 were component selective (Fig. 4). Within these populations, five (12%), seven (12%), and seven (17%) showed contrast-dependent phase-sensitive characteristics, respectively (Fig. 4, black symbols).

Fig. 4

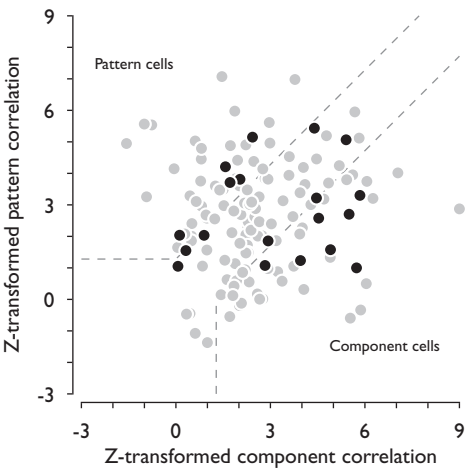

Pattern and component selectivity of cells in area MT. Scatter plot of *Z*-transformed pattern and component correlation for 138 complex cells in area MT. The dashed lines show the boundaries for reliable classification of pattern versus component selectivity. Complex cells that showed significant contrast-dependent phase sensitivity are shown in black; all other cells are shown in gray.

Discussion

In V1, we previously found that 44% of complex cells had contrast-dependent phase-sensitive characteristics, whereas in V2, only 7% of complex cells showed this property [5]. In V1, we suggested that as complex cells are only a few synapses away from the highly phase-selective responses of their primary feedforward inputs [e.g. neurons in the dorsal lateral geniculate nucleus (dLGN) or simple cells in the cortex], it might be that reducing contrast reduces the level of phase averaging to the point that phase-sensitive responses emerge [16,19,20]. Recurrent intracortical connections have a significant influence on response properties in V1 and these connections also likely influence the level of phase sensitivity (e.g. [21–24]). We argued that the additional layers of summation on the pathway to V2, with recurrent connectivity, were enough to prevent phase-sensitive responses from emerging at low contrast.

Here, we have shown that when contrast is reduced to just detectable levels, 14% of MT cells show increased phase sensitivity in response to moving gratings. The ranges of eccentricities for the V1, V2, and MT cells from which we have recorded are all restricted to the central visual field; thus, we do not believe that differences in eccentricity could account for the differences in the prevalence of contrast-dependent phase-sensitive cells between areas. It is difficult to assess the significance of the relatively small difference between the proportions of contrast-dependent phase-sensitive cells in V2 and MT (7 vs. 14%). However, there are clear differences between contrast-dependent cells in MT and V2. For the V2 cells, the mean F_1/F_0 measured at high contrast was 0.44, which places them in the upper tail of the V2 complex cell distribution (Fig. 3b, top). Given that the responses of these cells were already quite modulated at high contrast, it is not surprising that the modulation increased at low contrast, possibly because the underlying membrane potential modulation was close to the threshold. Conversely, the same cell type in MT had a much lower mean F_1/F_0 (0.13) when tested at high contrast, placing them at the peak of the MT cell distribution (Fig. 3a, top). Given that the responses of these MT cells were unmodulated at high contrast, it is noteworthy that one-seventh of them showed a significant increase in phase sensitivity at low contrast.

The functional plasticity in some MT neurons may be related to subcortical inputs from the dLGN and pulvinar. Area V2 receives most of its input from V1 [25], whereas area MT is more widely connected to cortical and subcortical brain regions. MT's main cortical inputs arise from V1, V2 and the dorsal area of V3 [8,26]. The input from V1 arises mainly from cells in layer 4B but also from the boundary between layers 5 and 6 [8,27–29]. These layers in V1 were found to have many complex cells that significantly increased phase sensitivity near their contrast threshold [5].

Cells projecting directly from V1 to MT are reported to be a specialized subset of V1 neurons: complex, highly direction selective, and sensitive to low stimulus contrast, which is relatively rare for V1 [29]. It is possible that the increase in response modulation that we observe in MT at low contrast reflects the sensitivity of these inputs from V1, which themselves may show contrast-dependent phase sensitivity. Magnocellular cells in the dLGN show greater sensitivity to low contrast than parvocellular cells [30]. MT's sensitivity to low contrasts may arise from a disproportionately large input from the M-pathway compared with V1 and V2. Given that the just detectable contrasts at which we measured increased phase sensitivity in MT were very low (Fig. 2), it implies M-pathway involvement.

However, a cortical hierarchical input organization cannot tell the whole story because inactivation of V1 does not completely remove the ability of MT neurons to respond to visual stimuli [10,31,32]. MT also receives input directly from subcortical brain regions. These include a disynaptic input from the retina through the koniocellular layers of the dLGN [33], a disynaptic input from the retina through the medial subdivision of the pulvinar [10], and a trisynaptic pathway from the retina through the superior colliculus and pulvinar [34]. It may be that some MT neurons have an underlying phase sensitivity that is derived from their direct subcortical inputs, which is only shown near their spiking threshold.

The RFs of neurons in V1 are small; thus, the neurons can only measure the component of the motion that moves orthogonal to the orientation of an edge [11]. Only being able to measure one component of the motion results in the ambiguity called the 'aperture problem' [7]. To overcome this problem, these initial motion signals are fed to neurons with larger RFs in MT [18]. About a third of MT neurons have the capacity to extract the direction of pattern motion, rather than just the motion orthogonal to local edges, whereas a third respond only to the component and the rest remain unclassified. We initially theorized that the component cells might be earlier in a hierarchical processing scheme within MT; thus, they might show increased levels of contrast-dependent phase sensitivity. However, we observed contrast-dependent phase sensitivity in roughly equal proportions among pattern and component neurons in MT. This last finding correlates with models suggesting that the processing of pattern direction in MT may not rely on a component-to-pattern cell hierarchy [11,12].

Acknowledgements

The authors thank J.A. Movshon (Centre for Neural Science, New York University, New York, New York, USA) in whose laboratory the recordings were performed.

S.L.C. and M.R.I. designed the research; S.L.C. and M.R.I. performed the research; S.L.C. contributed unpublished reagents/analytic tools; S.L.C. and M.R.I. analyzed data; and S.L.C. and M.R.I. wrote the paper.

This work was supported by the Australian Research Council (ARC) Centre of Excellence for Integrative Brain Function (CE140100007) and by the Victorian Lions Foundation that half funded S.L.C.'s fellowship.

Conflicts of interest

There are no conflicts of interest.

References

1 Skottun BC, de Valois RL, Grosof DH, Movshon JA, Albrecht DG, Bonds AB. Classifying simple and complex cells on the basis of response modulation. *Vision Res* 1991; **31**:1079–1086.
2 De Valois RL, Albrecht DG, Thorell LG. Spatial frequency selectivity of cells in macaque visual cortex. *Vision Res* 1982; **22**:545–559.
3 Levitt JB, Kiper DC, Movshon JA. Receptive-fields and functional architecture of macaque V2. *J Neurophysiol* 1994; **71**:2517–2542.
4 El-Shamayleh Y, Kumbhani RD, Dhruv NT, Movshon JA. Visual response properties of V1 neurons projecting to V2 in macaque. *J Neurosci* 2013; **33**:16594–16605.
5 Cloherty SL, Ibbotson MR. Contrast-dependent phase sensitivity in V1 but not V2 of macaque visual cortex. *J Neurophysiol* 2015; **113**:434–444.
6 Dubner R, Zeki SM. Response properties and receptive fields of cells in an anatomically defined region of the superior temporal sulcus in the monkey. *Brain Res* 1971; **35**:528–532.
7 Born RT, Bradley DC. Structure and function of visual area MT. *Annu Rev Neurosci* 2005; **28**:157–189.
8 Maunsell JHR, van Essen DC. The connections of the middle temporal visual area (Mt) and their relationship to a cortical hierarchy in the macaque monkey. *J Neurosci* 1983; **3**:2563–2586.
9 Livingstone MS, Pack CC, Born RT. Two-dimensional substructure of MT receptive fields. *Neuron* 2001; **30**:781–793.
10 Warner CE, Kwan WC, Wright D, Johnston LA, Egan GF, Bourne JA. Preservation of vision by the pulvinar following early-life primary visual cortex lesions. *Curr Biol* 2015; **25**:424–434.
11 Eskikand PZ, Kameneva T, Ibbotson MR, Burkitt AN, Grayden DB. A Possible role for end-stopped V1 neurons in the perception of motion: a computational model. *PLoS ONE* 2016; **11**:10.
12 Eskikand PZ, Kameneva T, Ibbotson MR, Burkitt AN, Grayden DB. A biologically-based computational model of visual cortex that overcomes the X-junction illusion. *Neural Netw* 2018; **102**:10–20.
13 Smith MA, Majaj NJ, Movshon JA. Dynamics of motion signaling by neurons in macaque area MT. *Nat Neurosci* 2005; **8**:220–228.
14 Ibbotson MR, Mark RF. Impulse responses distinguish two classes of directional motion-sensitive neurons in the nucleus of the optic tract. *J Neurophysiol* 1996; **75**:996–1007.
15 Ibbotson MR, Price NS, Crowder NA. On the division of cortical cells into simple and complex types: a comparative viewpoint. *J Neurophysiol* 2005; **93**:3699–3702.
16 Crowder NA, van Kleef J, Dreher B, Ibbotson MR. Complex cells increase their phase sensitivity at low contrasts and following adaptation. *J Neurophysiol* 2007; **98**:1155–1166.
17 Hietanen MA, Cloherty SL, van Kleef JP, Wang C, Dreher B, Ibbotson MR. Phase sensitivity of complex cells in primary visual cortex. *Neuroscience* 2013; **237**:19–28.
18 Movshon JA, Adelson EH, Gizzi MS, Newsome WT. The analysis of moving visual patterns. In: Chagas C, Gattass R, Gross C, editors. *Pattern recognition mechanisms*. New York, NY: Springer; 1985. pp. 117–151.
19 Meffin H, Hietanen MA, Cloherty SL, Ibbotson MR. Spatial phase sensitivity of complex cells in primary visual cortex depends on stimulus contrast. *J Neurophysiol* 2015; **114**:3326–3338.
20 van Kleef JP, Cloherty SL, Ibbotson MR. Complex cell receptive fields: evidence for a hierarchical mechanism. *J Physiol* 2010; **588**:3457–3470.
21 Chance FS, Nelson SB, Abbott LF. Complex cells as cortically amplified simple cells. *Nat Neurosci* 1999; **2**:277–282.
22 Tao L, Shelley M, McLaughlin D, Shapley R. An egalitarian network model for the emergence of simple and complex cells in visual cortex. *Proc Natl Acad Sci USA* 2004; **101**:366–371.
23 Wielaard DJ, Shelley M, McLaughlin D, Shapley R. How simple cells are made in a nonlinear network model of the visual cortex. *J Neurosci* 2001; **21**:5203–5211.

24 Zhu W, Shelley M, Shapley R. A neuronal network model of primary visual cortex explains spatial frequency selectivity. *J Comput Neurosci* 2009; **26**:271–287.
25 Lund JS. Anatomical organization of macaque monkey striate visual-cortex. *Annu Rev Neurosci* 1988; **11**:253–288.
26 Felleman DJ, van Essen DC. Distributed hierarchical processing in the primate cerebral cortex. *Cereb Cortex* 1991; **1**:1–47.
27 Shipp S, Zeki S. The organization of connections between areas V5 and V1 in macaque monkey visual-cortex. *Eur J Neurosci* 1989; **1**:309–332.
28 Tigges J, Tigges M, Anschel S, Cross NA, Letbetter WD, McBride RL. Areal and laminar distribution of neurons interconnecting the central visual cortical area-17, area-18, area-19, and area-mt in squirrel-monkey (Saimiri). *J Comp Neurol* 1981; **202**:539–560.
29 Movshon JA, Newsome WT. Visual response properties of striate cortical neurons projecting to area MT in macaque monkeys. *J Neurosci* 1996; **16**:7733–7741.
30 Usrey WM, Reid RC. Visual physiology of the lateral geniculate nucleus in two species of new world monkey: Saimiri sciureus and Aotus trivirgatis. *J Physiol* 2000; **523** (**Pt 3**):755–769.
31 Rodman HR, Gross CG, Albright TD. Afferent basis of visual response properties in area Mt of the macaque.I. Effects of striate cortex removal. *J Neurosci* 1989; **9**:2033–2050.
32 Girard P, Salin PA, Bullier J. Response selectivity of neurons in area MT of the macaque monkey during reversible inactivation of area V1. *J Neurophysiol* 1992; **67**:1437–1446.
33 Sincich LC, Park KF, Wohlgemuth MJ, Horton JC. Bypassing V1: a direct geniculate input to area MT. *Nat Neurosci* 2004; **7**:1123–1128.
34 Stepniewska I, Qi HX, Kaas JH. Projections of the superior colliculus to subdivisions of the inferior pulvinar in new world and old world monkeys. *Vis Neurosci* 2000; **17**:529–549.